

Article

Adaptation of a Cogenerator with Induction Generator to an On/Off-Grid Operation Using a Power Electronic System

Marian Kampik ¹, Marcin Fice ^{2,*} and Andrzej Jurkiewicz ³

¹ Department of Measurement Science, Electronics and Control, Faculty of Electrical Engineering, Silesian University of Technology, 44-100 Gliwice, Poland; marian.kampik@polsl.pl

² Energy Prosumer Section, Department of Electrical Engineering and Computer Science, Faculty of Electrical Engineering, Silesian University of Technology, 44-100 Gliwice, Poland

³ eGmina, Infrastruktura, Energetyka Sp. z o.o., 45-641 Opole, Poland; aj@egie.pl

* Correspondence: marcin.fice@polsl.pl

Abstract: Cogeneration sources play a very important role in the power industry with dispersed renewable sources with forced generation (e.g., photovoltaics and wind generators). They also fit into the circular economy by increasing the efficiency of fuel use, including biogas from agricultural or livestock waste. The aim of our research was to develop an effective source of electricity powered by agricultural biogas. The most important features of such a source are: operation in on-grid and off-grid mode, as well as a low cost of the device and uncomplicated operation. In addition, in Europe, the source of electricity connected to the power grid must meet the technical requirements of the “Network Codes Requirements for Generators” (NC RfG) network code. The appropriate certificate is easier to obtain using a power converter system for the source. For this purpose, an induction generator with a converter system and a small battery was planned. A converter system was developed and built, and then tests were carried out in various operating modes. During the measurements, it was confirmed that the requirements for the quality of electricity for off-grid and on-grid operation modes were met. The assumed maximum time of voltage recovery after changing the operating mode, amounting to 40 ms, was not exceeded. Furthermore, the limit values of phase voltages with unsymmetrical load, amounting to $\pm 10\%$ of the rated voltage, were not exceeded. In the battery usage off-grid mode, the time after a step change in the load power was not longer than 2 s.

Keywords: cogenerator; CHP; electronic power converter; induction generator; battery; on-grid; off-grid; EU network code NC RfG



Citation: Kampik, M.; Fice, M.; Jurkiewicz, A. Adaptation of a Cogenerator with Induction Generator to an On/Off-Grid Operation Using a Power Electronic System. *Appl. Sci.* **2023**, *13*, 5866. <https://doi.org/10.3390/app13105866>

Academic Editors: Levon Gevorkov and Olena Rubanenko

Received: 11 April 2023

Revised: 7 May 2023

Accepted: 8 May 2023

Published: 10 May 2023



Copyright: © 2023 by the authors. Licensee MDPI, Basel, Switzerland. This article is an open access article distributed under the terms and conditions of the Creative Commons Attribution (CC BY) license (<https://creativecommons.org/licenses/by/4.0/>).

1. Introduction

Distributed combined heat and power (CHP) generation on a small scale (mCHP—micro CHP) is part of the promotion of renewable energy [1], energy efficiency [2], and the circular economy, promoted by legal acts of the European Union (EU) [3]. Cogeneration systems up to 50 kW are dedicated to agricultural biogas plants installed in small or medium-sized agricultural and breeding farms. The potential for biogas (biomethane) production in Poland is 7 billion Nm³ per year [4]. These types of farms are located in rural areas surrounded by other buildings [5]. However, more and more often new breeding farms are launched away from buildings, e.g., because of the odor nuisance. In this case, building of a local energy source in the farm may turn out to be less costly than building a new power line. Such solutions can also act as a guaranteed power supply system. In Europe, internal combustion engines (ICE) are most commonly used for CHP propulsion [6]. This is because, among other things, controlling the generated power is relatively easy [7]. In addition, the use of an ICE as a driving source for CHP still seems to be the cheapest solution despite the continuous development of other types of drives based on micro gas turbines, micro Rankine cycle, Stirling, and thermophotovoltaic technologies [8], especially in the case of systems with power up to several dozen kilowatts [9]. This applies in particular to mCHP

technology. For farmers who operate and service agricultural machines on their own, a CHP operation built on a simple internal combustion engine is not difficult. For small CHPs, it is relatively easy to adjust the efficiency of the drive to match the system to the priority of electricity or heat [10], by controlling, for example, the rotational speed of the ICE [11,12].

1.1. Micro Electrical Systems with CHP

Micro power grids (micro electrical systems) have a great potential to become a solution to the electricity quality in power grids penetrated by micro renewable energy sources (micro-RES), especially photovoltaic sources with their own converter systems [13,14]. The influence of these sources is particularly visible in the values and shapes of voltages and currents in low-voltage (LV) grids. The solution may be an on-grid power system with its own control and balancing source. Such systems are connected to the power grid but are not visible to the active power (frequency) system control. This means that it balances the entire electrical energy demand in its own balancing shield (control shield, in particular an LV line). Renewable energy management in local LV grids usually uses the method of reducing the power generated from individual sources, to limit the voltage increase in the LV network and prevent the flow of energy to the medium-voltage (MV) grid [15]. There will be less and less sources with synchronous generators in the structures of microgrids powered by RES. This results in problems with ensuring sufficient system inertia for frequency control, especially in the case of micro systems covering a very small network area. Therefore, extensive frequency and voltage management systems in the LV network are necessary [16]. A good regulating and balancing source for local microgrids is a source driven by an ICE, i.e., a cogenerator. A good location for such a source is the LV grid on a farm with its own microbiogas power plant. The latter is not required if natural gas or other fuel is available.

1.2. Cogeneration Devices for Local Micro Electrical Systems

Typical solutions for regulation and balancing sources of electric energy are the use of synchronous generators connected to the power grid. Power converter systems are used more and more often to control power quality parameters in local microgrids. In local LV grids saturated with RES sources with their own inverters, there is a lack of kinetic energy stored in rotating machines. For such solutions, it is necessary to use connections that synchronize the operation of inverters in order to regulate the voltage and frequency [17,18]. This problem is particularly noticeable in a microgrid with one generator and a drive with a slight oversupply of torque (e.g., ICE). Frequency and voltage fluctuations may occur when the load power changes. The converter system, without kinetic energy resources, does not have sufficient control resources [19,20]. In such systems, it is necessary to use techniques to model hidden equivalent inertias for microgrids with RES using power converters [21–23]. A possible equivalent to complex control techniques is the use of local rotating sources together with small batteries, as shown later in this article.

Due to the low price, durability, and simplicity of the solution, induction machines driven by internal combustion engines are used for the construction of CHP generators and cogenerators up to 50 kW, fueled from microbiogas plants. For induction generators permanently connected to the grid, these solutions have been known for years [24]. However, the use of induction generators to supply the island network is associated with the problem of voltage regulation and excitation of the generator [25,26]. Cogeneration sources are currently treated as an excellent energy link in the circular economy. On the other hand, at the legislative level in the EU, they are a constantly underestimated flexible regulatory and balancing source [27–29]. Electrical power sources of up to 50 kW are formalized in Poland as prosumer energy sources [30]. Sources of up to 50 kW of electrical power can be connected to the grid on the basis of a notification submitted to the distribution system operator (DSO). The device must have a certificate confirming compliance with the technical requirements of the European NC RfG [31–33]. Induction generators are

also used in small-scale water and wind energy, but permanently connected to the power grid [34–36].

The mCHP devices typically operate connected to the power grid (on-grid), and for proper operation induction generators only require a capacitor bank compensating inductive reactive power. They are also adapted to work with constant power with the lowest specific fuel consumption [37,38]. This is quite a limitation, such a solution means that mCHP devices most often work in intermittent mode, i.e., they are switched on periodically during the day when the demand for energy is greater. However, an important advantage of induction generators is the lack of the need to use a power supply for the excitation winding [39]. There are solutions for coupling a DC source with a synchronous machine [40], but in the solution presented in this article it is necessary to use a battery to balance changes in the load power.

mCHP devices in the on-grid mode, although they have the ability to control the generated electric power by changing the fuel dose, are most often equipped with a manually controlled throttle and work with constant power. The manually controlled throttle reduces the cost of the device. However, such a system cannot properly generate energy in an off-grid installation without an excitation capacitance control system [41,42]. A major limitation in this case is also the low quality of electricity, especially large fluctuations in voltage and frequency [43]. Despite this, off-grid operation is increasingly required, e.g., in livestock farms requiring an emergency source of energy in the event of a power failure of the power grid.

Summing up the current state of the techniques used in practice to connect a source with an induction generator with a power of up to several dozen kilowatts:

- devices operating in on-grid and off-grid modes are built based on synchronous generators. The time of switching between on-grid and off-grid modes is not shorter than several seconds, which cannot be considered as an uninterruptible power supply;
- devices with induction generators operating in on-grid mode are permanently connected and usually operate with constant or variable electric power;
- converter systems are used to control the excitation of synchronous generators or in systems with induction generators as inverters, allowing the rotational speed of the generator and the driving internal combustion engine to be changed.

1.3. The Aim and the Scope of This Research Work

Power electronic converters are commonly used to control the parameters of electricity from a source connected to the grid [44]. The developed solution allows for uninterrupted generation of energy in on/off-grid modes, with the possibility of regulating the generated active power at the same time by changing the generator rotational speed and the fuel dose (torque of the driving engine), adjusting the operating point of the set to the lowest fuel consumption.

The battery in the off-grid mode provides the energy needed to excite the generator and regulate the voltage, and also provides energy during load power changes (it provides the equivalent of the power system inertia for frequency control). The time to take energy from the battery or give energy to the battery is relatively short, several seconds at maximum power (see Section 4). Therefore, the battery capacity is relatively small. In addition, such a solution allows for the introduction of a series of power types of cogeneration systems connected to the grid using one power converter system, in particular a converter connected to the power grid. This is important in the context of the NC RfG network code applicable in the European Union and the requirements for energy sources connected to the power grid. For practical reasons, for low-power sources, up to 50 kW, it is more cost-effective and less complicated to use a universal power converter system. It is also easier to fulfill the technical requirements, in accordance with the NC RfG, in the field of active and reactive power control in response to values of voltage and frequency in the network.

The main goal of this research work was to develop and build a power electronic system that would allow the cooperation of an induction generator driven by an internal

combustion engine with the low-voltage (LV) power grid (on-grid mode) and the island network (off-grid mode), with a power of up to 50 kW. For the construction of the power supply system, typical solutions of individual converters were used [45–48], but in a new topology, with the use of a small battery as a source of excitation of the induction generator and power balancing. In addition, the system should ensure almost uninterrupted switching between operating modes. For practical reasons, it was assumed that the switching time should not be longer than 40 ms. During this time, the voltage and frequency values must be restored. Uninterruptible switching between operating modes is necessary in the case of powering a farm that requires continuity of its energy supply.

It was assumed that the power supply system with an induction generator must fulfill the following technical requirements:

- in on-grid and off-grid modes, mCHP active power is controlled by changing the rotational speed and torque (e.g., fuel dose) of the internal combustion engine;
- in the off-grid mode, ensuring the quality parameters of electricity in accordance with the PN-EN 50160:2010E standard [49];
- switching time between modes < 40 ms.

Content of the article:

- the concept of the designed power supply system, its technical and functional requirements, as well as the topologies of the built power converters are presented in Section 2;
- a description of the tests carried out, as well as a description of the test stand and the devices used is presented in Section 3;
- the results of the experimental tests for the most important operating states are presented in Section 4.

2. Description of the Power Converter System Solution for a Cogenerator with an Induction Machine

A block diagram of the power supply system with an induction generator and a set of power converters is shown in Figure 1.

The characteristic feature of the system is the use of two AC–DC power converters (power grid PC2 and generator PC1) and one DC–DC battery converter with a dual-active-bridge (DAB) structure (PC3.1). In addition, a DC–DC buck–boost converter (PC3.2) was installed. PC3.2 discharges excess electricity when the battery voltage and current limits are reached during charging. The voltage of the DC bus between the converters is approx. 710 V. The nominal voltage of the battery is 48 V. The selected value of the battery voltage is due to practical reasons. The device will be operated by persons without appropriate qualifications to work on electrical installations. However, the user should be able to safely disconnect and reconnect the battery during routine service work. In on-grid mode, the DC bus voltage is stabilized by the PC2 grid converter, and the battery and PC3.1 and PC3.2 converters are not used. In the off-grid mode, the voltage on the DC bus is stabilized by the PC3.1 and PC3.2 power converters.

Assumed functional features of the power supply system with CHP:

- in on-grid and off-grid modes, power regulation at the grid connection point (on-grid) or load (off-grid) is carried out by changing the rotational speed of the induction generator (forced by the frequency of the voltage generated by the PC1 converter), controlling the dose of fuel (ICE) and the power of the electric energy storage;
- in on-grid and off-grid modes, the rotational speed of the induction machine can be changed within the permissible range, independent of the fixed voltage frequency in the power system. The rotational speed of the induction generator can be set by a generator converter, PC1. Then, the drive works with torque control (as it does in an internal combustion engine, by controlling the fuel dose);
- the possibility of supplying unbalanced three-phase loads [50].

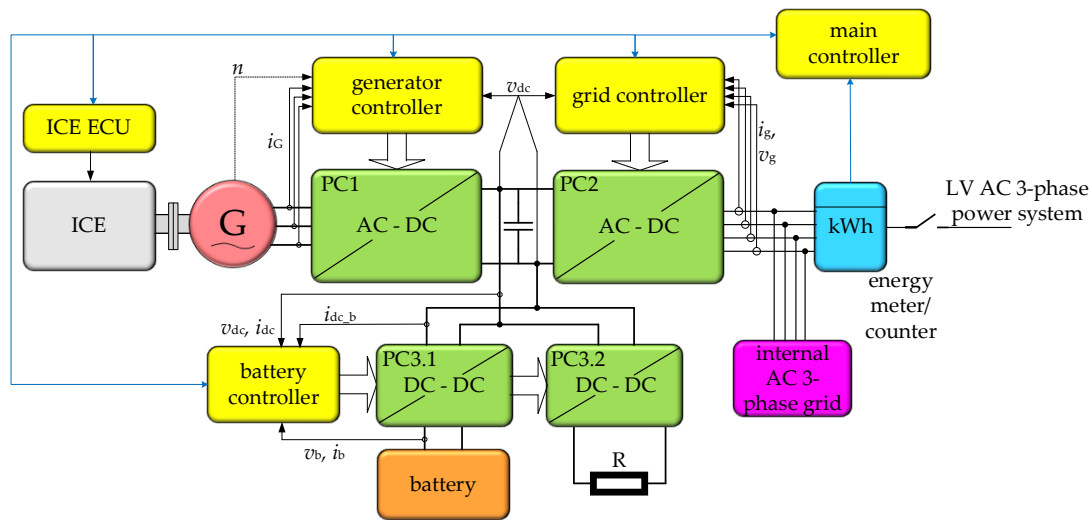


Figure 1. Block diagram of the designed power supply system with an ICE and an induction generator. ICE—internal combustion engine; G—induction generator; PC1—AC-DC power converter for induction generator; PC2—AC-DC power converter for AC grid; PC3.1—DC-DC DAB power converter for battery; PC3.2—DC-DC power converter for DC bus voltage limiting; R—load resistor; n —rotational velocity of induction generator; v_{dc} , i_{dc} —voltage and current of DC bus; i_G —phase current of generator; v_b , i_b —voltage and current of battery; v_g , i_g —voltage and current of grid. Source: author’s development.

2.1. Balancing Active Power in the Off-Grid Mode

Equipping the described power supply system with a power electronic converter allows for full use of the source properties in the regulation and balancing mode. A typical solution for a biogas micro power plant is the use of a cheap induction generator that requires a source of reactive power, usually a power supply network, to excite. In the case of connecting an induction generator with a power electronic converter and a battery, a source with adjustable active and reactive power, and the ability to operate in off-grid mode is obtained.

The basic balance of active power in the off-grid mode can be described by the equation:

$$\sum_{i=1}^k P_{s_i} = \sum_{j=1}^j P_{l_j} + \sum_{m=1}^m P_{b_m} \tag{1}$$

where P_{s_i} —active power of the energy source; P_{l_j} —active power of the load; and P_{b_m} —active power of the battery.

The power produced by the induction generator can be calculated as:

$$P_G = (T_{ICE} \cdot \omega) \eta_G \tag{2}$$

where T_G —torque of the ICE; ω —angular velocity; and η_G —efficiency of the induction generator.

In order to be able to continuously balance the active power using a cogenerator with an induction generator, the converter system is equipped with a battery. When the load power changes, additional energy is taken from the battery or transferred to the battery. To regulate the power of the power generator, the controller has two options: (1) changing the rotational speed of the generator, and (2) changing the torque by controlling the dose of fuel fed to the internal combustion engine. Figure 2 shows the characteristic operating states of the power supply system and the active power waveforms for: (1) steady state; (2) a stepwise reduction in load power; (3) a stepwise increase in the load power.

The time taken to establish a new operating point of the generator power system in response to a change in load power depends on: (1) the available battery power (and this depends on the capacity); (2) the throttle drive response time; (3) the oversupply of drive motor torque. The change in the drive power of the ICE can be forced in two ways: (1) a

change in the fuel dose; (2) a change in the rotational speed. It is possible (and desirable) to use both methods simultaneously in order to obtain the highest possible active power control dynamics.

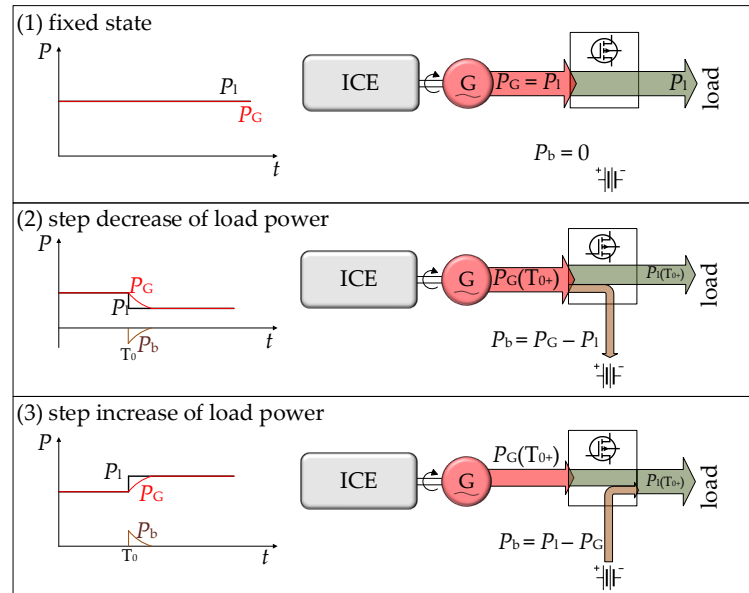


Figure 2. Supply system operating states. Source: author’s development.

The battery current can be controlled by controlling the torque (fuel dose control) and by changing the rotational speed:

$$(T_{ICE} \cdot \omega) \eta_G - P_l = (U_b \cdot I_b), \tag{3}$$

2.2. Topology of the Grid AC–DC Power Converter

The most commonly used two-level four-leg topology was selected for the construction of the PC2 power network converter. The four-leg topology is required due to the unbalanced load and the need to regulate the voltage in each phase separately. Figure 3 shows the selected topology of a four-leg DC–AC converter with an LCL filter and two contactors, ST1 and ST2. ST1 is the main contactor and ST2 is the starting contactor. An important feature of the four-leg converter is that the voltage in the DC circuit should exceed the value of the phase-to-phase voltage amplitude of the grid. Since the grid voltage amplitude is $\sqrt{2} \cdot 400 \text{ V} = 565 \text{ V}$, it is assumed that V_{dc} must be higher than 600 V.

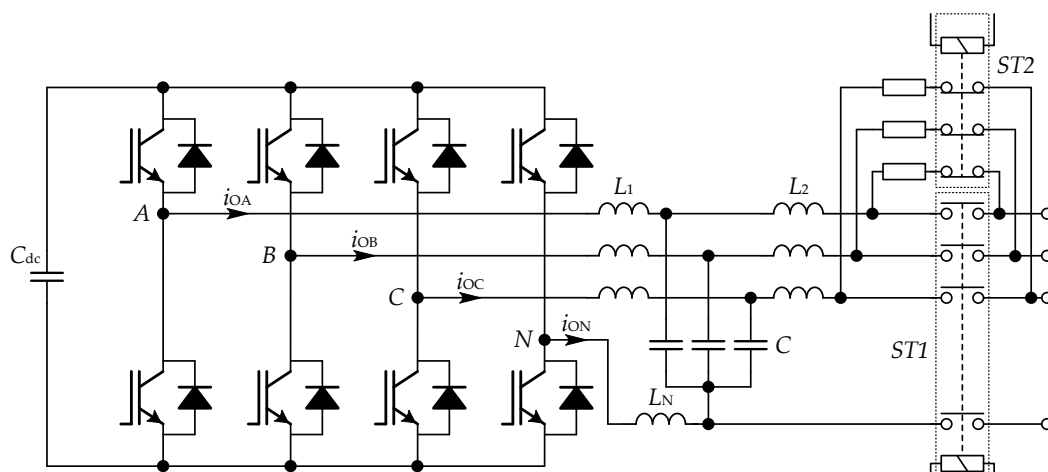


Figure 3. Scheme of a two-level, four-leg grid power converter. Source: author’s development.

IGBT power transistors, in the form of MB150BC120 IGBT half-bridges, were used in the prototype of the grid power converter. The transistor parameters were: maximum voltage 1200 V, maximum current 150 A.

2.3. Topology of the Generator AC–DC Power Converter

The most commonly used two-level three-leg topology was selected for the construction of the PC1 generator converter. The induction generator works with a symmetrical load; therefore, a three-leg topology was used. Figure 4 shows the selected topology of a three-leg DC–AC converter with an LCL filter and two contactors, ST1 and ST2. For a three-leg split capacitor converter, the V_{dc} voltage must be greater than twice the phase voltage amplitude. This means that $V_{dc} > 2\sqrt{2} 230 \text{ V} = 650.5 \text{ V}$. In practice, this voltage is set to approximately 700 V.

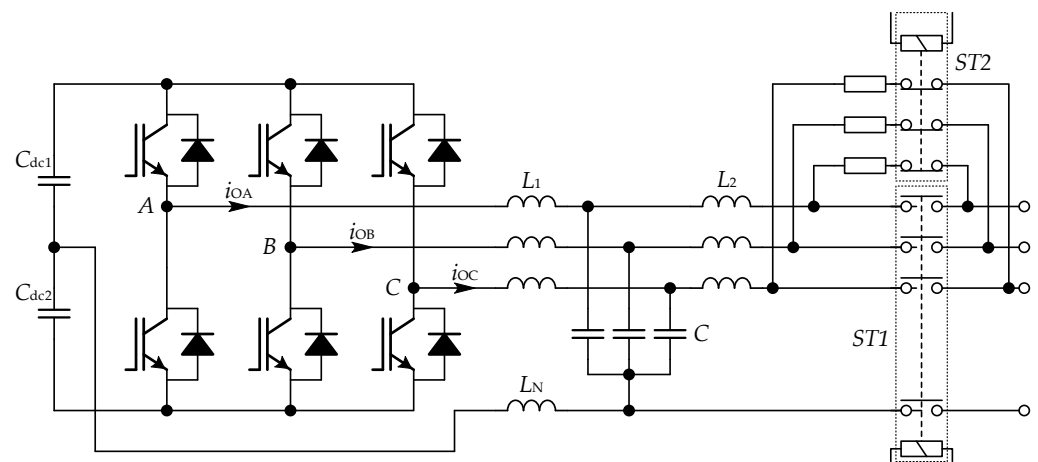


Figure 4. Scheme of a two-level, three-leg generator power converter. Source: author’s development.

IGBT power transistors, in the form of MB150BC120 IGBT half-bridges, were used in the prototype of the generator power converter. The transistor parameters were: maximum voltage 1200 V, maximum current 150 A.

2.4. Topology of the Battery DC–DC Power Converter

The battery converter is a bidirectional DC–DC converter, which is designed to convert the low voltage of the battery (48 V or more) into the DC circuit voltage of 600–800 V. The value of this voltage depends on the number of legs of the grid converter. Such a large voltage ratio ($700 \text{ V}/48 \text{ V} \approx 14.6$) makes the use of a bidirectional non-separated DC–DC buck–boost converter unjustified, due to the need to switch transistors with a very high duty cycle. A DAB converter was used in the project, a diagram of which is shown in Figure 5.

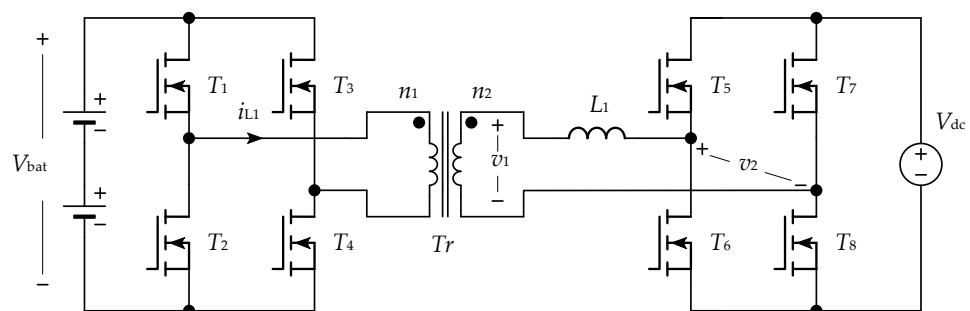


Figure 5. DAB DC–DC power converter. Source: author’s development.

On the low-voltage side (battery voltage) 150 V MOSFET transistors are used (IXFN400N15X3, IXYS Corporation, Milpitas, CA, USA). On the high-voltage side (DC bus voltage), IGBT transistors with a voltage class of 1200 V are used (FF50R12RT4, Infineon Technologies, Neubiberg, Germany). The turns ratio of the transformer, T_r , is $n_1/n_2 = 1/14.6$.

3. Materials and Methods

As part of the project, a prototype of the power converter system was built, consisting of four converters PC1, PC2, PC3.1, and PC3.2, lead–acid batteries with a capacity of 100 Ah and voltage of 48 V, and a Unitronics V700 programmable controller (V700-T20BJ, Unitronics, Israel). A prototype of a 20 kW converter system was built for tests. The power supply system was tested on a laboratory stand with an induction generator driven by an electric motor. The drive motor was powered by an inverter with adjustable speed or torque. During the tests, the torque was controlled by simulating a change in the throttle position of the ICE, and the rotational speed was controlled by the PC1 generator converter.

A scheme of the laboratory stand, with marked measurement points, is shown in Figure 6. A view of the measurement stand with the power electronic system installed in the cabinet is shown in Figure 7.

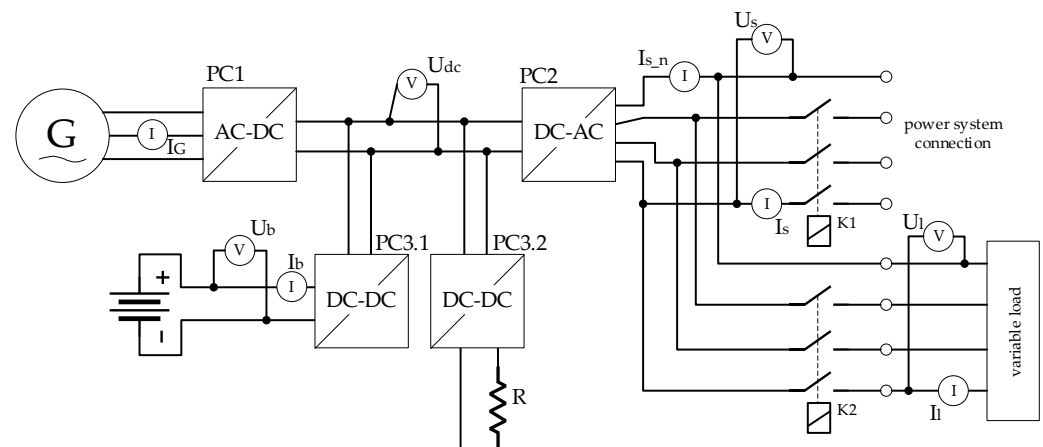


Figure 6. Scheme of the measuring setup with marked measuring points. Source: author’s development.



Figure 7. View of the measuring stand. Source: author’s development.

3.1. Laboratory Stand Equipment

Measuring instruments:

- Tektronix MDO3014 oscilloscope used in dynamic and transient states.

Voltage measurement accuracy: $\pm 1.5\%$ for 5 mV/div and above, derated at $0.1\%/^{\circ}\text{C}$ above 30°C $\pm 2.0\%$ for 2 mV/div, derated at $0.1\%/^{\circ}\text{C}$ above 30°C .

Time base accuracy: ± 10 ppm over any ≥ 1 ms interval.

Frequency measurement accuracy: $\pm([\text{Reference Frequency Error}] \times [\text{Marker Frequency}]) + (\text{span}/750 + 2)$ Hz; Reference Frequency Error = 10 ppm (10 Hz/MHz).

- FLUKE 435 analyzer of electric energy quality.

Power quality measurements: IEC61000-4-30 Compliance, Class A.

Voltage V_{rms} (AC + DC): $\pm 0.1\%$ of nominal voltage.

Current Arms (AC + DC): $\pm 0.5\% \pm 5$ counts.

Frequency: ± 0.01 Hz.

Watts (VA, W, var): $\pm 1\% \pm 10$ counts.

A block diagram of the test stand with the designation of the drive control systems (combustion engine simulator) and the generator (along with the converter system and the on/off-grid operating mode selector) is shown in Figure 8.

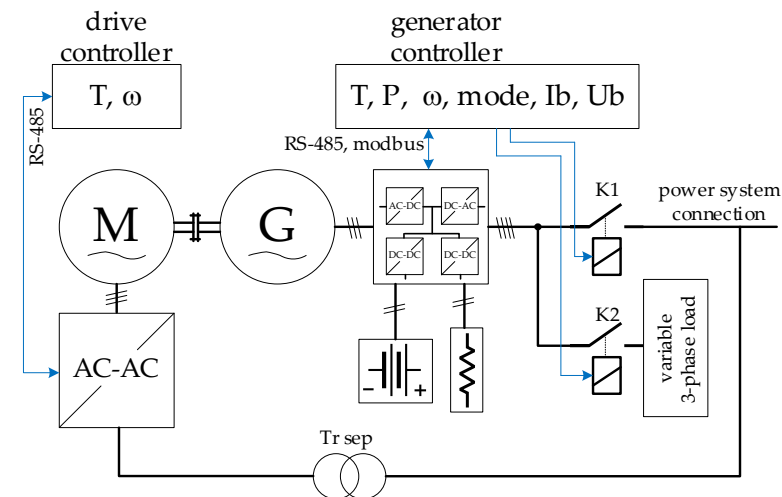


Figure 8. Block diagram of the test setup with the drive control system, the generator converter system, and the operating mode selector (on/off-grid). Source: author's development.

Equipment of the test stand:

- cabinet with built-in converters;
- a drive with an induction motor, M, and an inverter-diesel drive simulator;
- adjuster of generator G and drive system parameters;
- Load: (1) adjustable resistive unbalanced load with a power of 16.5 kW, consisting of 9 resistors with a power of approx. 2 kW each. The resolution of the load power regulation is approx. 0.5 kW for each phase separately. The load power value is true for the rated phase voltage of 230 V; (2) non-linear load: three-phase 6-pulse rectifier with resistive load.

The induction motor, M, was powered by an inverter. The inverter is controlled by specifying the torque or rotational speed of the motor. The generator converter system is controlled by setting the power at the connection to the network (only in on-grid mode), the load torque or the rotational speed of the induction generator G, as well as the on-grid or off-grid operating modes. It is also possible to limit battery current and voltage. The motor and the generator system are connected to the same grid, therefore, a separating transformer Tr_sep was used to power the drive motor.

3.2. Tests and Measurements Carried Out

In order to verify the adopted assumptions, the following tests and measurements of the power supply system with an induction generator and a converter system were carried out:

- on-grid operation: tests in the on-grid mode were aimed at checking the possibility of power control at the grid connection points. The generator control system stabilized the active power value at the grid connection by controlling the torque. The tests were carried out: (1) in a steady state for the maximum active power generated to the grid, without additional load and stabilization of the power value at the connection point (contactor K1 was on and K2 off); and (2) in a transient state during the change in resistive load (contactors K1 and K2 were on, during the measurement the value of the load power was changed by adding more resistors). In on-grid mode, the battery is not used. Power control was carried out at a constant rotational speed and variable torque;
- automatic switching between modes: the tests were aimed at measuring the value of the time of switching between the on-grid and off-grid modes during a power failure in the network (turning off the K1 contactor) and the appearance of voltage in the network (turning on the K1 contactor);
- off-grid operation: (1) measurements of the values of the generated phase voltages and active power at symmetrical and asymmetric resistive loads and non-linear loads; (2) measurements in transient states with changes in the load power values—during the tests, the load power values were changed step by step and the generator power regulation time and battery current were measured. The battery voltage and current limits were also tested.

Dynamic parameters of voltages and currents waveforms were measured using a Tektronix oscilloscope (e.g., switching and setpoint settling times). Electricity quality parameters (voltage, current and power values) were measured with a Fluke power quality analyzer. For the measurements carried out, the influence of the accuracy of the measuring instruments on the values of the generated voltage, current, and power was checked. Detailed information about the measurement procedures and results are provided in Section 4.

4. Results

In order to verify the assumptions as to the quality and functionality of the power supply system with an induction generator and a power converter system in on-grid and off-grid operating modes, a number of tests and measurements were carried out. The obtained results are presented, with a division into operating modes.

4.1. On-Grid Operation

To verify the correct operation of the power supply system various tests and measurements were performed. The tests were carried out by setting the generated power to the grid and switching on the receivers. The reaction to a power failure in the network and the transition to off-grid mode was also checked.

4.1.1. Generating a Constant Power

Measurements were carried out for several values of power generated in steady state. The results for the maximum power generated to the grid (about 20 kW) are presented below. The value of the active power generated to the grid is set in the controller just like the state of the contactor K1 (Figure 8), which is closed. The values of the currents and voltages (Figure 9) and the quality parameters of the electrical energy were measured in connection to the grid (Figures 10 and 11).

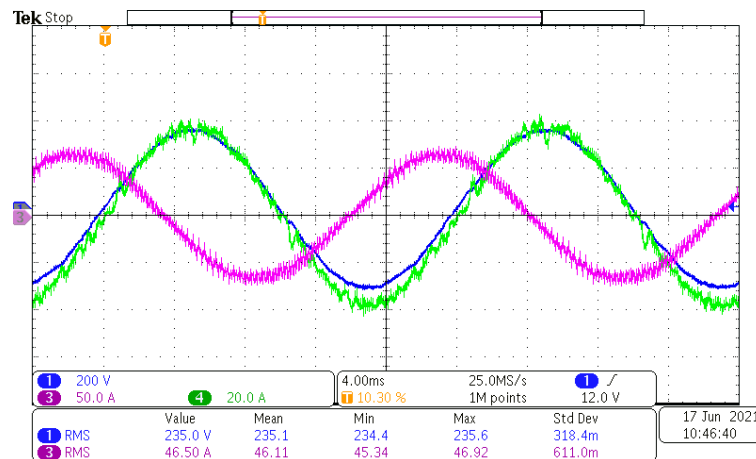


Figure 9. Waveforms of voltage, phase current, and generator current. The on-grid mode, generated power: 20 kW. 1—phase voltage; 3—phase current of the induction generator; 4—phase current on grid connection. Source: author’s development.

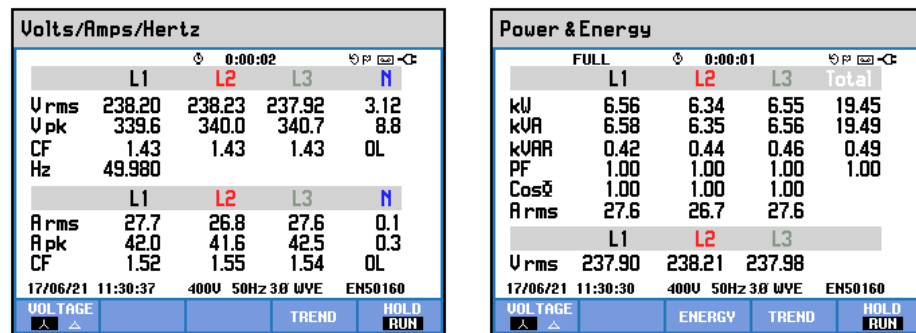


Figure 10. Values of phase voltages and currents, and power at the grid connection. The on-grid mode, generated power: 20 kW. Source: author’s development.

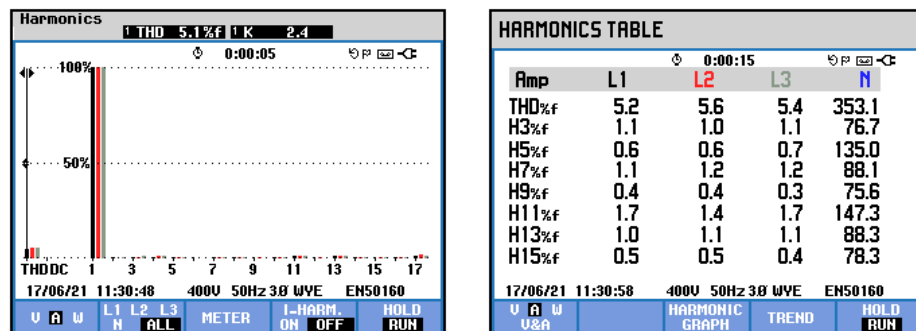


Figure 11. Current harmonics. The on-grid mode, generated power: 20 kW. Source: author’s development.

For the Fluke manufacturer’s stated measurement accuracies, the measured values are: (1) voltage of phase L1: 238.20 ± 0.23 V; (2) current of phase L1: 27.6 ± 0.6 A; (3) active power of phase L1: 6.56 ± 0.1 kW.

4.1.2. Step Change in Load Power

The tests were aimed at checking the possibility of regulating the generator power during a step change in the load power in the on-grid mode. The control is based on the signal from the measurement system installed at the connection point to the grid. The current waveforms and voltages during the test are shown in Figures 12 and 13.

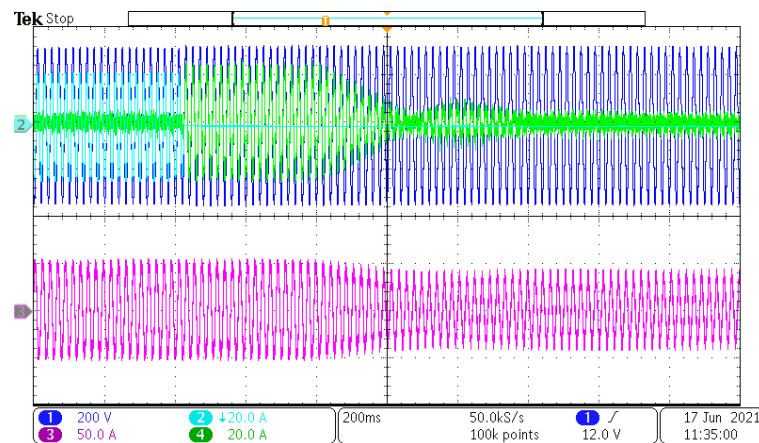


Figure 12. Voltage and current waveforms when 12 kW load is switched on. ①—grid phase voltage; ②—load phase current; ③—generator phase current ④—grid phase current. Source: author's development.

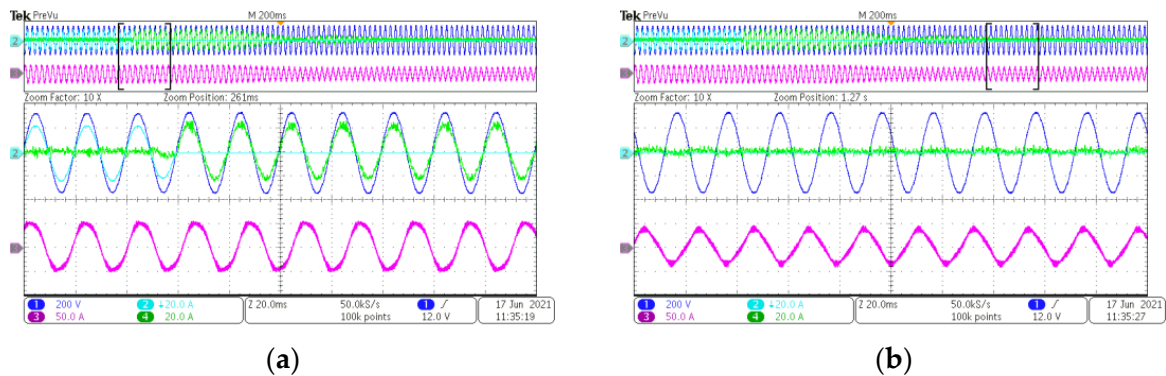


Figure 13. Waveforms of voltage and current during switching on the 12 kW load (enlargement of fragments of waveforms in Figure 12): (a) switching on the load; (b) reducing the connection power to zero. ①—grid phase voltage; ②—load phase current; ③—generator phase current ④—grid phase current. Source: author's development.

In the on-grid mode, power regulation takes place without the participation of the battery. Tests were carried out with a change in the torque of the drive motor and a constant rotational speed stabilized by a generator converter. The aim was to reduce the power at the point of connection to the grid to zero. After switching on the 12 kW load, the torque of the drive motor was increased (at constant rotational speed) until the active power at the connection point was equal to 0. The time to obtain a new operating point does not exceed 2 s.

The increase in the current consumption from the power grid is shown in Figure 13a. There is a gradual increase in the torque of the drive motor until the power at the connection is reduced to zero (Figure 13b).

4.1.3. Switching between Operating Modes

The test of switching between the operating modes consisted in switching between the grid supply and the island with a non-linear load connected (resistive load connected through a six-pulse rectifier). Power failure was simulated by opening the K1 contactor. The restoration of the supply voltage was simulated by turning on the contactor K2.

The voltage and current waveforms of one load phase and the voltage controlling the switching contactor were recorded (Figure 14—switching to off-grid mode, Figure 15—switching to on-grid mode). The voltage waveform of the contactor K1 allows one to assess the speed of operation of the contactor itself, which affects the time of physical switching between operating modes.

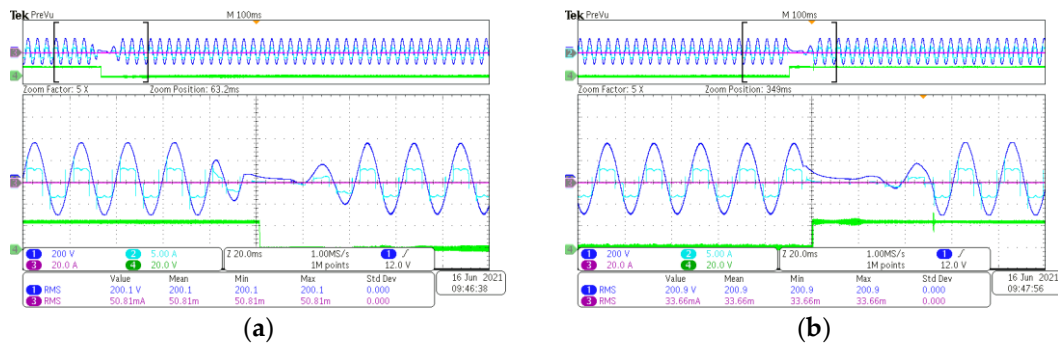


Figure 14. Load voltage and phase current waveforms: (a) on-grid → off-grid; (b) off-grid → on-grid. ①—phase voltage; ②—phase current; ③—not connected; ④—voltage of the K1 contactor. Source: author’s development.

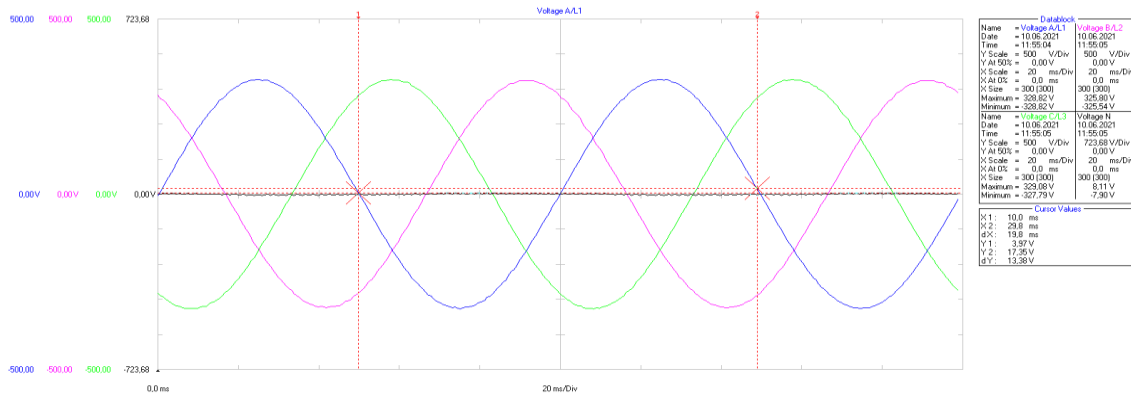


Figure 15. Waveforms of phase voltages of the receiver for a symmetrical load, power 20 kW. Source: author’s development.

Taking into account the time of switching on the voltage supplying the contactor after the failure and the return of the grid voltage, the switching time is shorter than 20 ms. The voltage is restored in approx. 40 ms.

4.2. Off-Grid Operation

Several tests and measurements were carried out to verify the correct operation of the power supply system, the quality parameters of electricity, and the dynamics of regulation at variable load power and various types of loads (symmetrical, asymmetric and non-linear).

4.2.1. Symmetric Load in Steady States

Measurements of electric energy quality parameters in a steady state were performed by measuring the phase voltages and currents of a symmetrical resistive load. The measurement results for a 3 × 5.5 kW load are shown below. The load power values are true for a rated phase voltage of 230 V. The waveforms of the phase voltages are shown in Figure 15. The values of power, RMS phase voltages, and voltage harmonics are shown in Figure 16. The voltage asymmetry is shown in Figure 17.

For the Fluke manufacturer’s stated measurement accuracies, the measured values are: (1) voltage of phases L1: 230.77 ± 0.23 V, L2: 229.20 ± 0.23 V, L3: 230.97 ± 0.23 V; (2) active power of phases L1: 5.54 ± 0.1 kW, L2: 5.52 ± 0.1 kW, L3: 5.62 ± 0.1 kW.

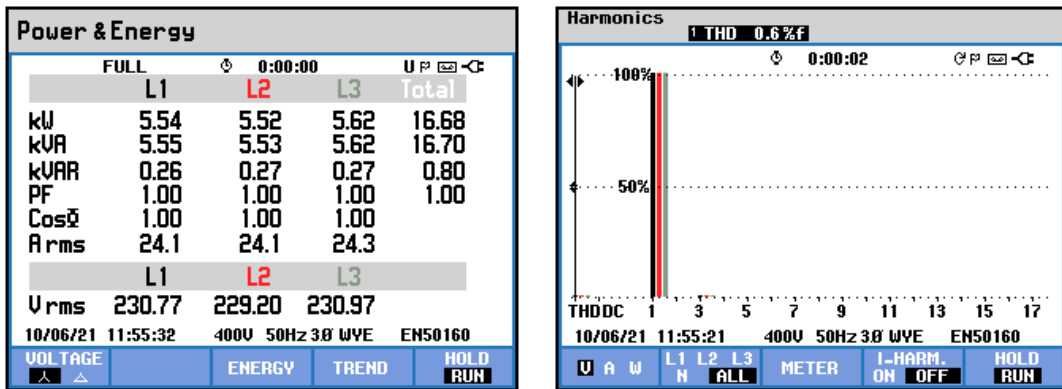


Figure 16. Phase load power values, root mean square (RMS) values of phase voltages and voltage harmonics. Off-grid mode, symmetrical load. The colors of the lines in the harmonics diagram represent the individual phases. Source: author’s development.

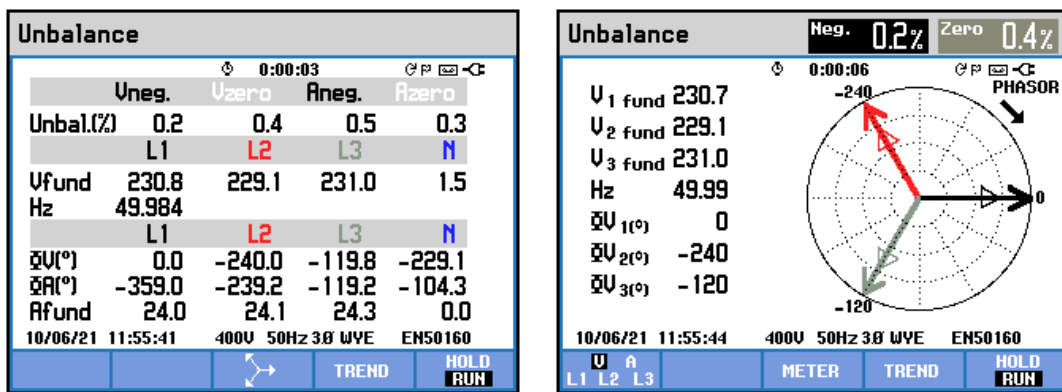


Figure 17. Phase voltage unbalance. Off-grid mode, symmetrical load. The colors of the arrows in the unbalance diagram represent the individual phases. Source: author’s development.

4.2.2. Unsymmetrical Load in Steady States

Measurements of electric energy quality parameters in a steady state were carried out by measuring the phase voltages and currents of an unsymmetrical resistive load. The measurement results for the phase loads 5.5 kW, 5.5 kW, 0 kW are shown in the figures below. The waveforms of phase voltages and values of phase voltages and currents are shown in Figure 18. The power values and voltage harmonics are shown in Figure 19. The voltage asymmetry is shown in Figure 20.

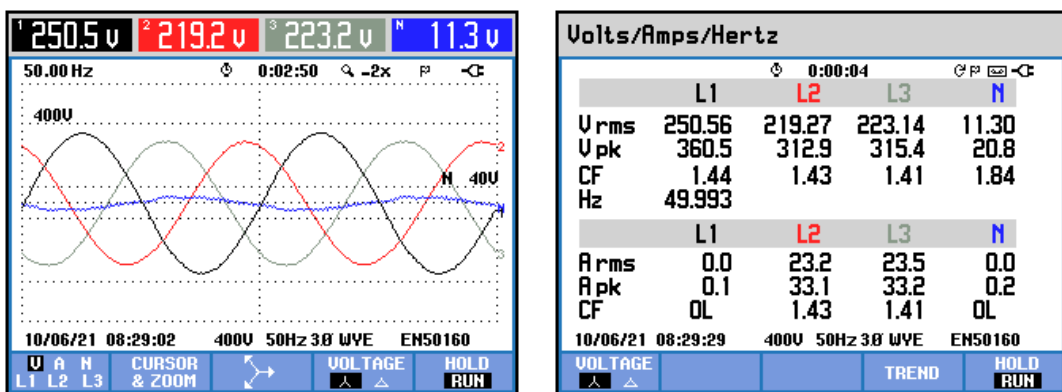


Figure 18. Waveforms and values of phase voltages and currents. Off-grid mode, unsymmetrical load. Source: author’s development.

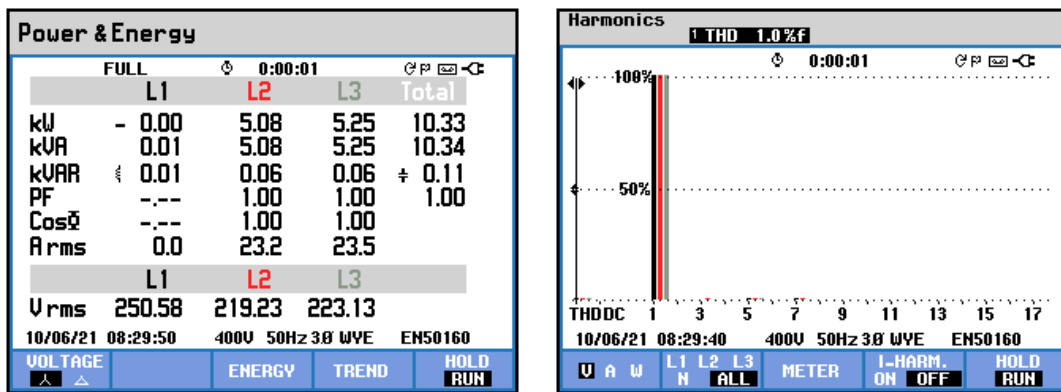


Figure 19. Load power values and voltage harmonics. Off-grid mode, unsymmetrical load. The colors of the lines in the harmonics diagram represent the individual phases. Source: author’s development.

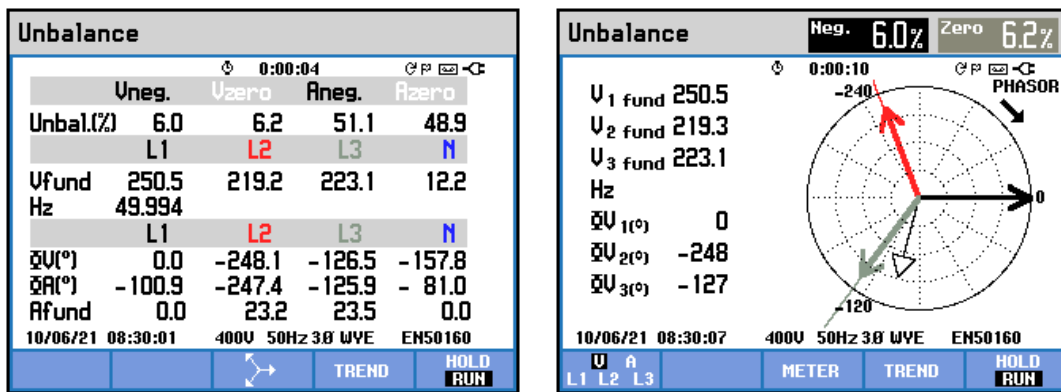


Figure 20. Phase voltage unbalance. Off-grid mode, unsymmetrical load. The colors of the arrows in the unbalance diagram represent the individual phases. Source: author’s development.

The most important result of the test was checking the asymmetry of the phase voltages. The voltage values in individual phases did not exceed the permissible values $\pm 10\%$ of the rated value. For a rated voltage of 230 V the permissible range is 207–253 V. For a resistive load, there is only one basic harmonic.

For the Fluke manufacturer’s stated measurement accuracies, the measured values are: (1) voltage of phases L1: 250.56 ± 0.23 V, L2: 219.27 ± 0.23 V, L3: 223.14 ± 0.23 V; (2) current of phases L1: 0, L2: 23.2 ± 0.6 A, L3: 23.5 ± 0.6 A; (3) active power of phases L1: 0, L2: 5.08 ± 0.1 kW, L3: 5.25 ± 0.1 kW. In this example, the effect of the voltage value on the active power of a resistive load can be seen.

4.2.3. Non-Linear Symmetrical Load in Steady States

Measurements of electric energy quality parameters in a steady state were carried out by measuring the phase voltages and currents of a symmetric non-linear load. A resistive load connected through a six-pulse rectifier was used for the tests. The measurement results for a 5 kW load are shown below. The waveforms of the phase voltages and currents are shown in Figure 21. The load power, phase voltages, and currents are shown in Figure 22. The voltage and current harmonics are shown in Figures 23 and 24, respectively.

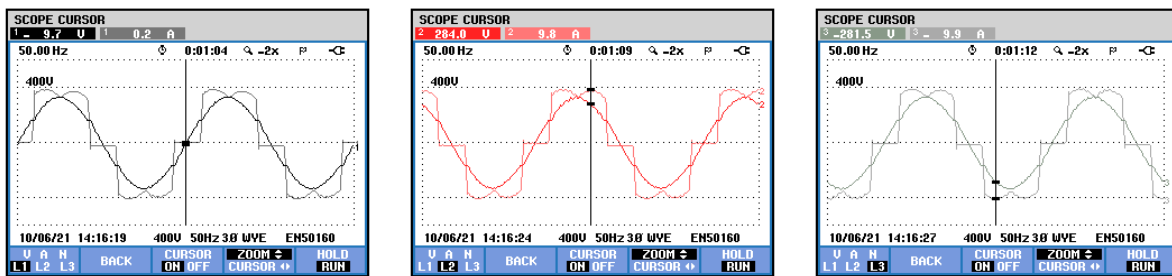


Figure 21. Waveforms of voltages and currents in individual phases. Off-grid mode, non-linear symmetrical load. Source: author’s development.

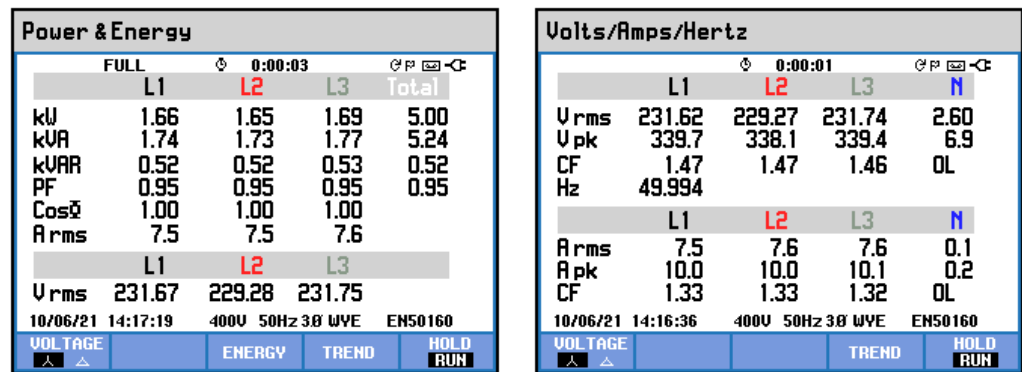


Figure 22. Values of load power, phase voltages, and currents of the load. Off-grid mode, non-linear symmetrical load. Source: author’s development.

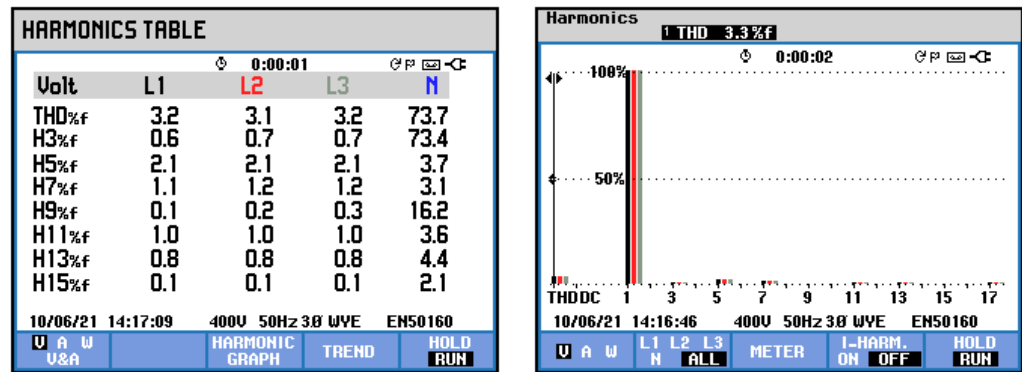


Figure 23. Voltage harmonics. Off-grid mode, non-linear symmetrical load. The colors of the lines in the harmonics diagram represent the individual phases. Source: author’s development.

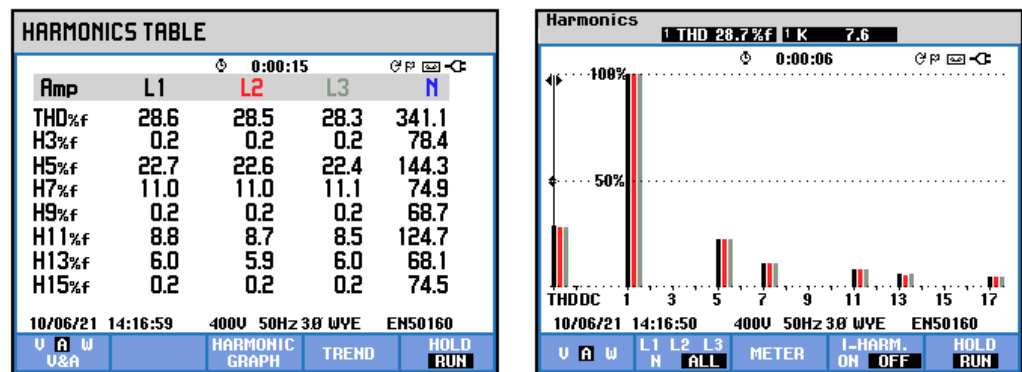


Figure 24. Current harmonics. Off-grid mode, non-linear symmetrical load. The colors of the lines in the harmonics diagram represent the individual phases. Source: author’s development.

For the Fluke manufacturer's stated measurement accuracies, the measured values are: (1) voltage of phases L1: 231.62 ± 0.23 V, L2: 229.27 ± 0.23 V, L3: 231.74 ± 0.23 V; (2) current of phases L1: 7.5 ± 0.6 A, L2: 7.6 ± 0.6 A, L3: 7.6 ± 0.6 A; (3) active power of phases L1: 1.66 ± 0.1 kW, L2: 1.65 ± 0.1 kW, L3: 1.69 ± 0.1 kW.

The most important result of the test was to check the harmonics of the generated voltage for a non-linear load. For the connected load—a resistor connected through a six-pulse rectifier—the current harmonics are shown in Figure 24. For this load, the generated voltage waveform contains small harmonic values. However, there is a constant component, approx. 3%.

4.3. Off-Grid Operation—Dynamic Parameters during Load Power Changes

Tests in transient states during load power change—switching on and off the load—were carried out. The following values were measured: load phase current (to determine the moment of load power change), load phase voltage, battery voltage and current, and DC bus voltage. The tests were carried out in two variants: (1) without changing the generator operating point and; (2) with changing the rotational speed of the generator in order to adjust the generated power to the load power and reduce the battery current.

4.3.1. Parameter Measurements in the DC Circuit, Operation without Power Control of the Induction Generator

During operation without power control of the induction generator, any change in load power is balanced by the battery. The battery charging current was limited to 40 A and the discharge current to 150 A.

Switching on the 9.5 kW Load

The battery current was initially set at 40 A, charging with a power of approx. 2 kW. The generator works with a constant power of approx. 4 kW. The surplus power from the generator is redirected to the resistor using the PC3.2 converter. The battery current, load current, DC bus voltage, and battery voltage waveforms are shown in Figure 25.

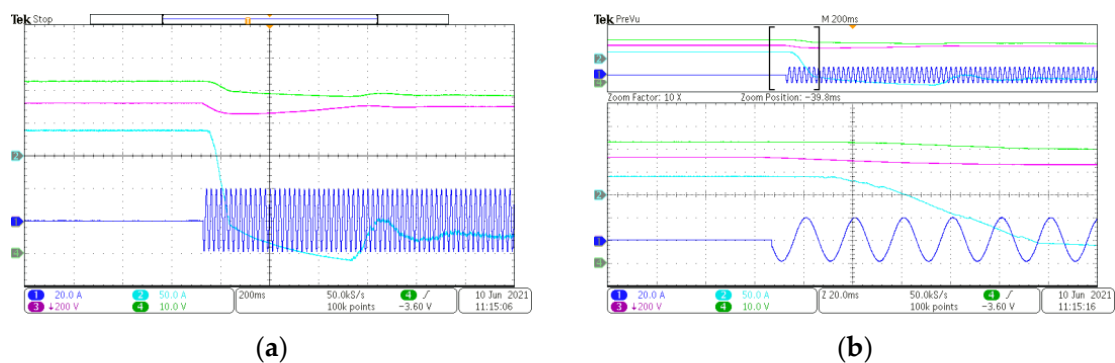


Figure 25. Turning on a 9.5 kW load in off-grid mode, with constant generator power: (a) current and voltage waveforms; (b) enlarged fragment of waveforms from Figure 25a during load switching. ①—load phase current; ②—battery current; ③—DC bus voltage; ④—battery voltage. Source: author's development.

After switching on the receiver, the battery current changed the direction of flow (discharge) and stabilized at a value of approx. 120 A, after rebuilding the voltage in the DC circuit (710 V). The time taken to restore the DC voltage was approx. 600 ms.

Switching off the 9.5 kW Load

The battery current is initially set to 0 A. The generator power is also 0. Waveforms of the battery current, load current, DC bus voltage, and battery voltage are shown in Figure 26.

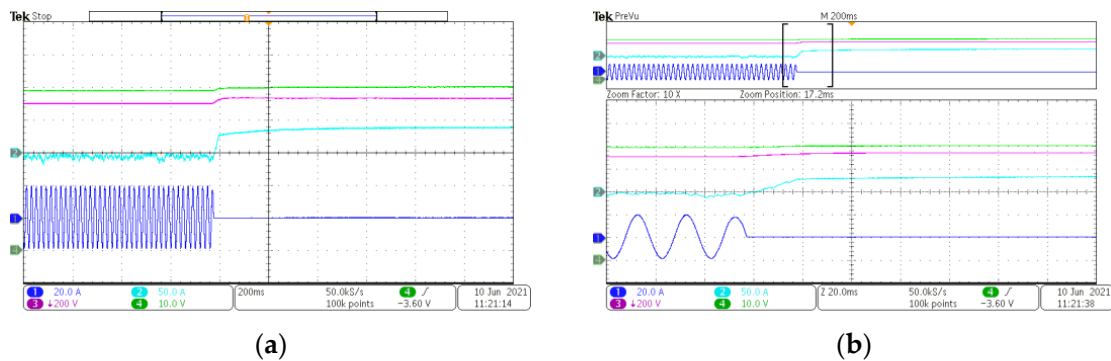


Figure 26. Turning off a 9.5 kW load in off-grid mode, with constant generator power: (a) current and voltage waveforms; (b) enlarged fragment of waveforms from Figure 26a during load switching. ①—load phase current; ②—battery current; ③—DC bus voltage; ④—battery voltage. Source: author’s development.

After the receiver, the battery current increased to approximately 40 A (maximum charging value). Then, the PC3.2 converter turned on, redirecting the surplus power to the resistor and stabilizing the DC link voltage to a value of approx. 730 V.

4.3.2. Measurements of Parameters in the DC Circuit, Operation with Power Control of the Induction Generator

The power control of the induction generator was carried out by controlling its rotational speed. In this mode, the drive motor operates with a constant torque. The speed control system is designed to control the battery current. After the load power, the set value of the rotational speed changes, which corresponds to a battery current of 0 A. The rotational speed is represented in the figures below by the waveform of the generator current, on which the frequency change is visible.

Switching on and off the 5.5 kW Load

Waveforms of the voltages and currents during the switching on and off of a 5.5 kW load are shown in Figure 27. Before starting the test, the generator speed controller set the rotational speed for which the battery current was approx. 0 A. Then, after changing the load power, the controller set the rotational speed for which the battery current was approx. 0 A again. The tests made it possible to set the parameters of the regulator in such a way that the time of re-establishing the set value of the battery current was approx. 2 s.

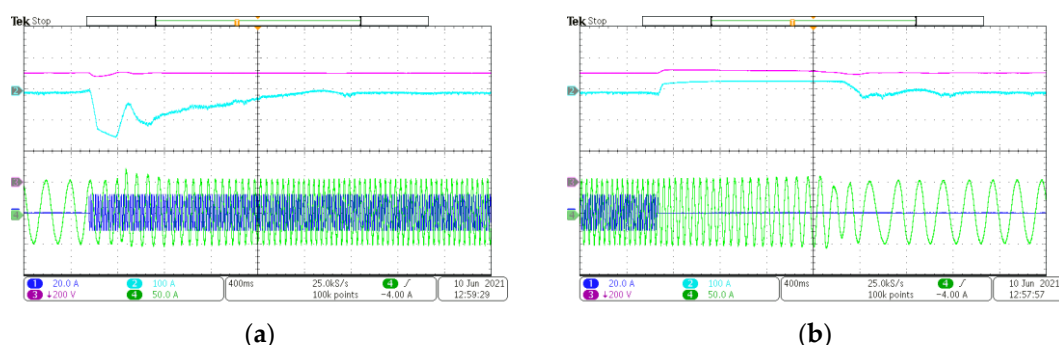


Figure 27. Off-grid operation with 5.5 kW load power changes and regulated generator power: (a) turning on a load; (b) turning off a load. ①—load phase current; ②—battery current; ③—DC bus voltage; ④—induction generator current. Source: author’s development.

4.3.3. Battery and DC Circuit Limit Tests

Measurements were carried out in the off-grid mode to test the operation of the DC circuit. In the off-grid mode, the voltage of the DC circuit is stabilized by the PC3.1 and

PC3.2 converters. The PC3.1 converter is the source of energy for the DC circuit in order to maintain the set voltage of approx. 710 V. If the battery cannot receive the voltage of the surplus energy, the voltage of the DC circuit increases. With an excessive increase in the DC bus voltage (above 720 V), the PC3.2 converter is switched on, transferring the surplus energy to the resistor, R. When the load power increases, the battery is the source of energy for the DC bus, until a new operating point of the drive motor is established. The voltage and current waveforms in the DC circuit when the 8.5 kW load is switched on are shown in Figure 27. The AC output voltage of the converter system is shown in Figure 28. The load voltage is shown in Figure 28. Before switching on the load, the battery current was set to 0 A, the output power of the power supply system was also approx. 0 W (the generator power covered the needs of the power supply system).

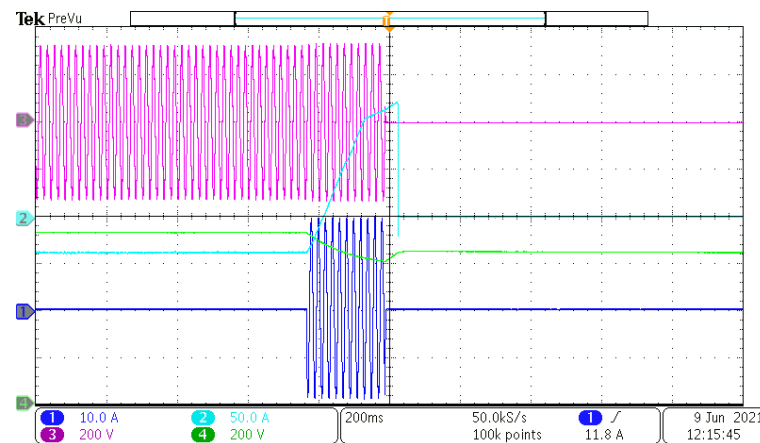


Figure 28. Off-grid operation, switching on a load with a power of 8.5 kW. **1**—load phase current; **2**—battery current; **3**—output AC voltage; **4**—DC bus voltage. Source: author’s development.

Figures 28 and 29 show that after about 200 ms the output voltage supplying the receivers was turned off. The battery current increased to approximately 160 A and the DC bus voltage decreased to the limit of 600 V. The PC2 grid converter turned off. The battery current waveform consists of two straight lines, inclined at different angles. The first angle depends on the inductance of the transformer circuit of the DAB converter. After approximately 120 ms, the battery current increase ramp was limited to a safe value for the battery circuit, to protect against exceeding the maximum current. After approx. 160 ms, the current has not yet reached its maximum value (165 A), but the voltage in the DC link has decreased to approx. 600 V and the PC2 grid converter has switched off. For the next 40 ms, the current was discharged the battery to rebuild the voltage on the DC bus. After exceeding the maximum value of the battery current, the converter was turned off. The rise time of the battery current is decisive for the maximum power obtained from the battery, because during this time the voltage in the DC link decreases. The second factor is the voltage of the battery. For a nominal voltage of 48 V (lead–acid battery), the discharge voltage may drop to 40 V. The final charging voltage is approx. 56 V.

The waveforms of the voltages and currents when a load of approximately 6.5 kW was switched on are shown in Figure 30.

A step change in the load power of approx. 6.5 kW, with an average battery voltage of approx. 42 V, did not cause the DC bus voltage to drop below 600 V. The energy drawn from the DC circuit capacitors was compensated by the battery current after approx. 180 ms. Then the DC bus voltage was restored to approx. 710 V.

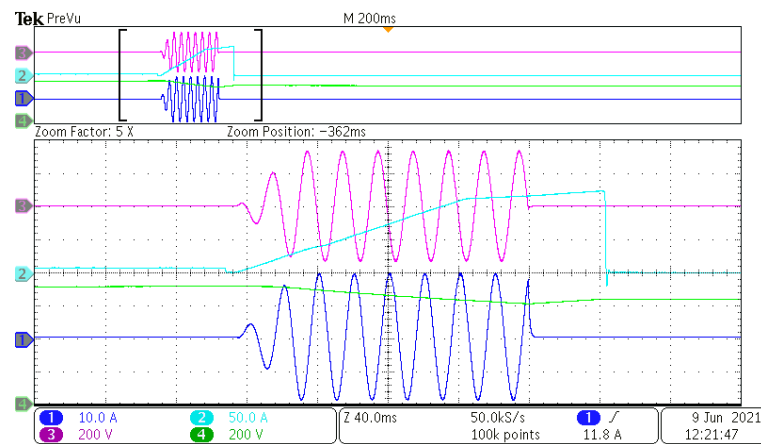


Figure 29. Off-grid operation, switching on a load with power of 8.5 kW. **1**—load phase current; **2**—battery current; **3**—load voltage; **4**—DC bus voltage. Source: author’s development.

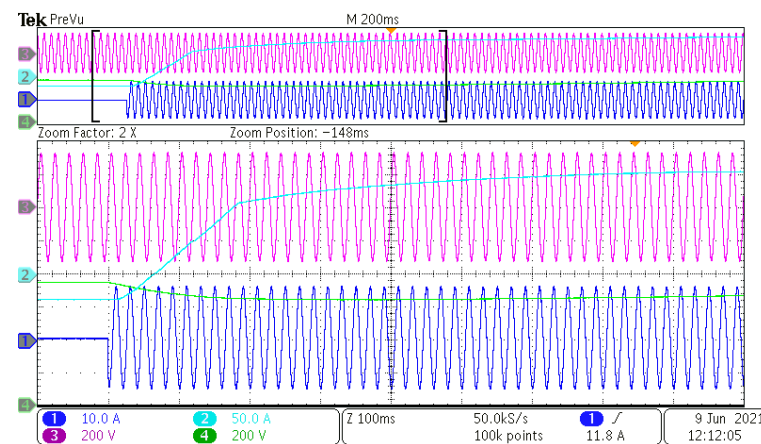


Figure 30. Off-grid operation, switching on a load with power of 6.5 kW. **1**—load phase current; **2**—battery current; **3**—output AC voltage; **4**—DC bus voltage. Source: author’s development.

5. Discussion

The results of the laboratory tests carried out confirmed the achievement of the required quality parameters of electricity within the adopted range. Particularly important is the time to switch between on/off-grid modes, which does not exceed 20 ms. Furthermore, the values of phase voltages in the off-grid mode with unbalanced load do not exceed the permissible values ($\pm 10\% U_n$).

During the tests, the problem of limitations related to the DC bus and the battery in off-grid mode when changing the load power became apparent. Power limitation during a step load change results from the instantaneous battery voltage and the maximum discharge current, as well as from the current rise time in the DAB converter. The current rise time is mainly due to the inductance of the transformer and the parasitic inductance of the DC circuit. The transformer ratio was selected for the rated voltage of the battery, i.e., 48 V, and the voltage of the DC circuit (approx. 700 V) and was equal to approximately 14 V/V. In order to minimize the current rise time, it was necessary to limit the number of turns. With a small number of turns of the primary winding, the range of changes in the ratio is relatively large. For the built prototype, the range of step power change at which the DC bus voltage will be restored, depending on the voltage at the battery terminals (40–48 V during discharge), is 6.6–8 kW. Above this value, the PC2 grid converter will switch off. The use of a 48 V battery for higher load power is unjustified, because the increase in current will complicate the power electronics system. Therefore, for higher power it will be

necessary to increase the DC bus voltage. This will also allow the use of a simpler PC3.1 converter circuit in the buck–boost topology.

6. Conclusions

The complexity of the power converter system for a cogenerator and adding a battery may seem unjustified and expensive. However, looking at the whole solution, the built power supply system has advantages that the conventional solution does not have, i.e., the possibility of cooperation with the grid and uninterrupted transition to an off-grid power supply. In a typical solution, additional battery systems (uninterruptible power supplies, UPS) are used. The assumption was to use a battery of small capacity, sufficient for temporary power balancing in transients. At the same time, it is possible to use a high-capacity battery which serves as a guaranteed power supply system when, for example, the generator drive is stopped.

The use of the power converter system allows the building of a universal and scalable power supply system with an induction generator, because the NC RfG certificate will be issued only for the network converter. Other converters will be adapted to the power of the generator as well as the capacity and power of the battery.

State of achievements of main assumptions:

- in on-grid and off-grid modes, mCHP active power is controlled by changing the rotational speed and torque (e.g., fuel dose) of the internal combustion engine.

This assumption was tested in a simulation with an electric motor instead of an ICE. Based on the obtained results, shown in Sections 4.1 and 4.2, it can be concluded that active power controlled by torque or rotational speed provides sufficient dynamics. Determination of the set active power at the connection point with the grid did not exceed 2 s;

- in the off-grid mode, ensuring the quality parameters of the electricity in accordance with the PN-EN 50160:2010E standard.

In this case, voltage stabilization in off-grid mode is important. The values of the phase voltages with an asymmetric load did not exceed the permissible values. The obtained extreme values of phase voltages were about 251 V and 219 V.

- switching time between modes < 40 ms.

The switching time between operating modes was approx. 20 ms.

Feature work: in the next stage of the prototype development of the power supply system, the characteristics of the output power as a function of frequency and grid voltage will be implemented in order to meet the requirements of the NC RfG network code. The use of an additional PC3.2 converter also improves the dynamics of power balance control in the on-grid mode (e.g., limiting the power at the connection to the power grid). In the finished product, a heater is planned to be connected to the heat recovery circuit of the internal combustion engine. The heater will act as an additional resistor, R . The use of a converter system to stabilize the off-grid parameters allows for the connection of other energy sources, e.g., a photovoltaic source, which requires stable voltage parameters in the installation to which it is connected. This functionality will also be tested in the next stage of prototype testing.

7. Patents

Patent application at the Patent Office of the Republic of Poland under the number P.441476.

Author Contributions: Conceptualization, M.F. and A.J.; methodology, M.F.; validation, M.F.; formal analysis, M.K.; investigation, M.F.; resources, A.J.; data curation, M.F.; writing—original draft preparation, M.F.; writing—review and editing, M.K.; visualization, M.F.; supervision, M.K.; project administration, A.J.; funding acquisition, A.J. All authors have read and agreed to the published version of the manuscript.

Funding: This research was funded by the European Regional Development Fund within the Regional Operational Program of the Opolskie Voivodeship, for the years 2014–2020, grant number RPOP.01.01.00-16-0017/18.

Institutional Review Board Statement: Not applicable.

Informed Consent Statement: Not applicable.

Data Availability Statement: Data can only be made available on the basis of an individual request to the authors of the article. The data are not publicly available.

Conflicts of Interest: The authors declare no conflict of interest.

Nomenclature

Acronyms:

AC	Alternate current
CHP	Combined heat and power
DC	Direct current
DAB	Dual-active-bridge
ECU	Electronic control unit
G	Generator
ICE	Internal combustion engine
K	Contactora
LV	Low-voltage grid
M	Motor
mCHP	Micro CHP
MV	Medium-voltage grid
NC RfG	Network Code on Requirements for Generators
RES	Renewable energy source
RMS	Root Mean Square

Symbols:

C	Capacitor
i, I	Current
L	Coil
P	Power
PC1	AC–DC power converter for induction generator
PC2	AC–DC power converter for AC grid
PC3.1	DC–DC DAB power converter for battery
PC3.2	DC–DC power converter for DC bus voltage limiting
R	resistor
u, U	Voltage
ω	Angular velocity

Subscripts:

ac	Alternate current
b	Battery
dc	Direct current
G	Generator
g	Grid
l	Load
OA	Phase A leg
OB	Phase B leg
OC	Phase C leg
N	Neutral
T	Torque
η	Efficiency
ω	Angular velocity

References

1. Directive (EU) 2018/2001 of the European Parliament and of the Council of 11 December 2018 on the Promotion of the Use of Energy from Renewable Sources (Recast). 2018. Available online: https://eur-lex.europa.eu/legal-content/EN/TXT/?uri=uriserv:OJ.L_.2018.328.01.0082.01.ENG&toc=OJ:L:2018:328:TOC (accessed on 20 January 2023).
2. European Union. The European Green Deal. Available online: https://ec.europa.eu/info/strategy/priorities-2019-2024/european-green-deal_en (accessed on 16 January 2023).
3. European Union. *Circular Economy Action Plan*; Technical Report; Publications Office of the European Union: Luxembourg, 2020.
4. *National Energy and Climate Plan for the Years 2021–2030*; Technical Report; Ministry of Climate and Environment: Warsaw, Poland, 2019.
5. Piechota, G.; Igliński, B. Biomethane in Poland—Current Status, Potential, Perspective and Development. *Energies* **2021**, *14*, 1517. [[CrossRef](#)]
6. Martinez, S.; Michaux, G.; Salagnac, P.; Bouvier, J.-L. Micro-combined heat and power systems (micro-CHP) based on renewable energy sources. *Energy Convers. Manag.* **2017**, *154*, 262–285. [[CrossRef](#)]
7. Amidpour, M.; Manesh, M.H.K. Chapter 9—Cogeneration and polygeneration targets. In *Cogeneration and Polygeneration Systems*; Amidpour, M., Manesh, M.H.H., Eds.; Elsevier Academic Press: London, UK, 2021; pp. 137–161.
8. Vishwanathan, G.; Sculley, J.P.; Fischer, A.; Zhao, J.-C. Techno-economic analysis of high-efficiency natural-gas generators for residential combined heat and power. *Appl. Energy* **2018**, *226*, 1064–1075. [[CrossRef](#)]
9. Barbieri, E.S.; Spina, P.R.; Venturini, M. Analysis of innovative micro-CHP systems to meet household energy demands. *Appl. Energy* **2012**, *97*, 723–733. [[CrossRef](#)]
10. Caresana, F.; Brandoni, C.; Feliciotti, P.; Bartolini, C.M. Energy and economic analysis of an ICE-based variable speed-operated micro-cogenerator. *Appl. Energy* **2011**, *88*, 659–671. [[CrossRef](#)]
11. Angrisani, G.; Roselli, C.; Sasso, M. Distributed microtrigeneration systems. *Prog. Energy Combust. Sci.* **2012**, *38*, 502–521. [[CrossRef](#)]
12. De Paepe, M.; D’Herdt, P.; Mertens, D. Micro-CHP systems for residential applications. *Energy Convers. Manag.* **2006**, *47*, 3435–3446. [[CrossRef](#)]
13. Karimi, M.; Mokhlis, H.; Naidu, K.; Uddin, S.; Bakar, A.H.A. Photovoltaic penetration issues and impacts in distribution network—A review. *Renew. Sustain. Energy Rev.* **2016**, *53*, 594–605. [[CrossRef](#)]
14. Kharrazi, A.; Sreeram, V.; Mishra, Y. Assessment techniques of the impact of grid-tied rooftop photovoltaic generation on the power quality of low voltage distribution network—A review. *Renew. Sustain. Energy Rev.* **2020**, *120*, 109643. [[CrossRef](#)]
15. Li, Y.; Nejabatkhah, F. Overview of control, integration and energy management of microgrids. *J. Mod. Power Syst. Clean Energy* **2014**, *2*, 212–222. [[CrossRef](#)]
16. Tayyebi, A.; Groß, D.; Anta, A.; Kupzog, F.; Dörfler, F. Frequency Stability of Synchronous Machines and Grid-Forming Power Converters. *IEEE J. Emerg. Sel. Top. Power Electron.* **2020**, *8*, 1004–1018. [[CrossRef](#)]
17. Unruh, P.; Nuschke, M.; Strauß, P.; Welck, F. Overview on Grid-Forming Inverter Control Methods. *Energies* **2020**, *13*, 2589. [[CrossRef](#)]
18. Fernández-Guillamón, A.; Gómez-Lázaro, E.; Muljadi, E.; Molina-García, Á. Power systems with high renewable energy sources: A review of inertia and frequency control strategies over time. *Renew. Sustain. Energy Rev.* **2019**, *115*, 109369. [[CrossRef](#)]
19. Abazari, A.; Dozein, M.G.; Monsef, H. A New Load Frequency Control Strategy for an AC Micro-grid: PSO-based Fuzzy Logic Controlling Approach. In Proceedings of the 2018 Smart Grid Conference (SGC), Sanandaj, Iran, 28–29 November 2018; pp. 1–7.
20. Gu, H.; Yan, R.; Saha, T.K. Minimum Synchronous Inertia Requirement of Renewable Power Systems. *IEEE Trans. Power Syst.* **2018**, *33*, 1533–1543. [[CrossRef](#)]
21. Blaabjerg, F.; Chen, Z.; Kjaer, S.B. Power electronics as efficient interface in dispersed power generation systems. *IEEE Trans. Power Electron.* **2004**, *19*, 1184–1194. [[CrossRef](#)]
22. Blaabjerg, F.; Iov, F.; Kerekes, T.; Teodorescu, R.; Ma, K. Power electronics—Key technology for renewable energy systems. In Proceedings of the 2nd Power Electronics, Drive Systems and Technologies Conference, Tehran, Iran, 16–17 February 2011; pp. 445–466.
23. Carrasco, J.M.; Franquelo, L.G.; Bialasiewicz, J.T.; Galván, E.; PortilloGuisado, R.C.; Prats, M.M.; Leon, J.I.; Moreno-Alfonso, N. Power-electronic systems for the grid integration of renewable energy sources: A survey. *IEEE Trans. Ind. Electron.* **2006**, *53*, 1002–1016. [[CrossRef](#)]
24. de Mello, F.P.; Feltes, J.W.; Hannett, L.N.; White, J.C. Application of induction generators in power systems. *IEEE Trans. Power App. Syst.* **1982**, *PAS-101*, 3385–3393. [[CrossRef](#)]
25. Parsons, J.R., Jr. Cogeneration application of induction generators. *IEEE Trans. Ind. Appl.* **1984**, *IA-20*, 497–503. [[CrossRef](#)]
26. Murthy, S.S.; Malik, O.P.; Tandon, A.K. Analysis of self excited induction generators. *Inst. Electr. Eng. Proc. C Gener. Transmiss. Distrib.* **1982**, *129*, 260–265. [[CrossRef](#)]
27. De Souza, R.; Casisi, M.; Micheli, D.; Reini, M. A Review of Small–Medium Combined Heat and Power (CHP) Technologies and Their Role within the 100% Renewable Energy Systems Scenario. *Energies* **2021**, *14*, 5338. [[CrossRef](#)]
28. Hammond, G.P.; Tittley, A.A. Small-Scale Combined Heat and Power Systems: The Prospects for a Distributed Micro-Generator in the ‘Net-Zero’ Transition within the UK. *Energies* **2022**, *15*, 6049. [[CrossRef](#)]

29. Alanne, K.; Saari, A. Sustainable small-scale CHP technologies for buildings: The basis for multi-perspective decision-making. *Renew. Sustain. Energy Rev.* **2004**, *8*, 401–431.
30. Polish Regulations: Act of 20 February 2015 on Renewable Energy Sources (JoL of 2022 Item 1378, as Amended). Available online: <https://isap.sejm.gov.pl/isap.nsf/DocDetails.xsp?id=WDU20150000478> (accessed on 20 January 2023).
31. Commission Regulation (EU) 2016/631 of 14 April 2016 Establishing a Network Code on Requirements for Grid Connection of Generators (NC RfG). 2016. Available online: https://eur-lex.europa.eu/legal-content/EN/TXT/?uri=OJ%3AJOL_2016_112_R_0001 (accessed on 20 January 2023).
32. Chmielowiec, K.; Topolski, L.; Piszczek, A.; Hanzelka, Z. Photovoltaic Inverter Profiles in Relation to the European Network Code NC RfG and the Requirements of Polish Distribution System Operators. *Energies* **2021**, *14*, 1486. [[CrossRef](#)]
33. Bollen, M.H.J.; Hassan, F. *Integration of Distributed Generation in the Power System*; John Wiley & Sons, Inc.: Hoboken, NJ, USA, 2011.
34. Chen, Z.; Guerrero, J.M.; Blaabjerg, F. A Review of the State of the Art of Power Electronics for Wind Turbines. *IEEE Trans. Power Electron.* **2009**, *24*, 1859–1875. [[CrossRef](#)]
35. Nababan, S.; Muljadi, E.; Blaabjerg, F. An overview of power topologies for micro-hydro turbines. In Proceedings of the 2012 3rd IEEE International Symposium on Power Electronics for Distributed Generation Systems (PEDG), Aalborg, Denmark, 25–28 June 2012; pp. 737–744.
36. Singh, R.R.; Chelliah, T.R.; Agarwal, P. Power electronics in hydro electric energy systems—A review. *Renew. Sustain. Energy Rev.* **2014**, *32*, 944–959. [[CrossRef](#)]
37. Caliano, M.; Bianco, N.; Graditi, G.; Mongibello, L. Economic optimization of a residential micro-CHP system considering different operation strategies. *Appl. Therm. Eng.* **2016**, *101*, 592–600. [[CrossRef](#)]
38. Bianchi, M.; De Pascale, A.; Ruggero Spina, P. Guidelines for residential micro-CHP systems design. *Appl. Energy* **2012**, *97*, 673–685. [[CrossRef](#)]
39. Kroposki, B.; Pink, C.; DeBlasio, R.; Thomas, H.; Simões, M.; Sen, P.K. Benefits of power electronic interfaces for distributed energy systems. *IEEE Trans. Energy Convers.* **2010**, *25*, 901–908. [[CrossRef](#)]
40. Can, E.; Sayan, H.A.S.A.N. PID and fuzzy controlling three phase asynchronous machine by low level DC source three phase inverter. *Teh. Vjesn.-Tech. Gaz.* **2016**, *23*, 753–760.
41. Bansal, R.C. Three-phase self-excited induction generators: An overview. *IEEE Trans. Energy Convers.* **2005**, *20*, 292–299. [[CrossRef](#)]
42. Tandon, A.K.; Murthy, S.S.; Berg, G.J. Steady State Analysis of Capacitor Self-Excited Induction Generators. *IEEE Trans. Power Appar. Syst.* **1984**, *PAS-103*, 612–618. [[CrossRef](#)]
43. Al-Bahrani, A.H.; Malik, N.H. Voltage control of parallel operated self excited induction generators. *IEEE Trans. Energy Convers.* **1993**, *8*, 236–242. [[CrossRef](#)]
44. Souza Junior, M.E.T.; Freitas, L.C.G. Power Electronics for Modern Sustainable Power Systems: Distributed Generation, Microgrids and Smart Grids—A Review. *Sustainability* **2022**, *14*, 3597. [[CrossRef](#)]
45. Rocabert, J.; Luna, A.; Blaabjerg, F.; Rodriguez, P. Control of power converters in AC microgrids. *IEEE Trans. Power Electron.* **2012**, *27*, 4734–4749. [[CrossRef](#)]
46. Katiraei, F.; Iravani, R.; Hatziargyriou, N.; Dimas, A. Microgrids management. *IEEE Power Energy Mag.* **2008**, *6*, 54–65. [[CrossRef](#)]
47. Coelho, E.A.A.; Cortizo, P.C.; Garcia, P.F.D. Small-signal stability for parallel-connected inverters in stand-alone AC supply systems. *IEEE Trans. Ind. Appl.* **2002**, *38*, 533–542. [[CrossRef](#)]
48. Can, E. The design and experimentation of the new cascaded DC-DC boost converter for renewable energy. *Int. J. Electron.* **2019**, *106*, 1374–1393. [[CrossRef](#)]
49. *EN 50160:2010*; European Standard Voltage Characteristics of Electricity Supplied by Public Electricity Networks. CENELEC: Brussels, Belgium, 2010.
50. Pena, R.; Cardenas, R.; Escobar, E.; Clare, J.; Wheeler, P. Control System for Unbalanced Operation of Stand-Alone Doubly Fed Induction Generators. *IEEE Trans. Energy Convers.* **2007**, *22*, 544–545.

Disclaimer/Publisher’s Note: The statements, opinions and data contained in all publications are solely those of the individual author(s) and contributor(s) and not of MDPI and/or the editor(s). MDPI and/or the editor(s) disclaim responsibility for any injury to people or property resulting from any ideas, methods, instructions or products referred to in the content.